Single-cell dissection of plasma cell clonal evolution to smoldering multiple myeloma after CD19 CAR-T cell therapy in B-cell acute lymphoblastic leukemia

Chimeric antigen receptor T (CAR-T) cell therapy has revolutionized the treatment of B-cell malignancies, achieving deep and durable remissions in patients with B-cell acute lymphoblastic leukemia (B-ALL).[1] Despite remarkable therapeutic successes, rare but clinically significant secondary hematologic malignancies have been reported during CAR-T cell therapy, often driven by lineage switching or clonal selection.[2] Moreover, CAR-T cell therapy drives profound remodeling of the immune microenvironment, and the sustained inflammatory signaling may promote clonal evolution and influence disease progression.[3] High-resolution approaches, such as single-cell RNA sequencing (scRNA-seq) and single-cell B-cell receptor sequencing (scBCR-seq), enable characterization of transcriptional programs, clonal identity, and temporal dynamics to dissect CAR-T cell therapy-induced clonal evolution and immune remodeling.[4]

Here, we report a case of B-ALL with B-cell receptor (BCR) heterogeneity at diagnosis that evolved into smoldering multiple myeloma (SMM) following CD19-targeted CAR-T therapy. The co-occurrence of B-ALL and SMM is exceptionally rare, as it requires malignant clones at distinct stages of B-cell development. This case provides a unique opportunity to dissect how CAR-T cell therapy drives B-lineage clonal evolution and reshapes the immune microenvironment. To this end, bone marrow mononuclear cells (BMMNC) were collected at multiple time points and subjected to longitudinal scRNA-seq and scBCR-seq to track dynamic changes in malignant and immune cell populations, thereby elucidating the mechanisms of clonal evolution and immune remodeling following CAR-T cell therapy. The patient gave informed consent and was enrolled in a clinical trial registered at clinicaltrials.gov (Identifier: NCT00123456). The study was approved by the Ethics Committee of the Institute of Hematology & Blood Diseases Hospital CAMS&PUMC (IIT2024019-EC-1).

The clinical course of this 58-year-old patient is illustrated in Figure 1A, and key clinical parameters are summarized in Figure 1B. Initial bone marrow smear showed 96.5% lymphoblasts and 0.5% plasma cells. Immunophenotyping revealed 84.02% abnormal B lymphoblasts expressing CD19, cCD79a, CD10, TdT, HLA-DR, and CD38, with partial expression of CD34 and CD20. Cytogenetics identified t(9;22)(q34.1;q11.2) and *BCR*::*ABL1* p210 fusion. Ig gene rearrangement detected two clonal immunoglobulin kappa deletion-elements (IGKDE), one clonal immunoglobulin heavy chain (IGH), and two clonal immunoglobulin lambda light chain (IGL) rearrangements. After three cycles of VOVP chemotherapy[5] followed by blinatumomab, the patient achieved complete remission (CR) with undetectable measurable residual disease (MRD) by flow cytometry. Next-generation sequencing (NGS)-based MRD tracking showed a significant decrease and eventual disappearance of IGKDE clones, while IGH and IGL clones increased (Figure 1C).

Given persistent NGS-based MRD positivity, indicating a potentially poor prognosis,[6] the patient received CD19 CAR-T cell therapy (murine-derived, second-generation, 4-1BB co-stimulatory domain, FMC63 scFv). CAR-T cells reached peak expansion on day 9 post-infusion (Figure 1D). On day 28 post-infusion, B-ALL blasts were eradicated, while plasma cells rose to 20% (Figure 1B), with persistent IGH and IGL clones (Figure 1C). Serum IgG rose to 40.10 g/L, with gradual increase in total globulin, and the differential free light chain (dFLC, |κ-FLC – λ-FLC|) was 56.75 mg/L. Bone marrow biopsy showed 10-20% abnormal plasma cells. Immunophenotyping identified 1.5% abnormal plasma cells expressing CD138, CD56, CD38, CD200, CD27, and cytoplasmic λ, with weak CD81, CD45, CD117, and CD28, and absent CD19/CD20/cytoplasmic κ. No radiological evidence of bone destruction was detected. Fluorescence *in situ* hybridization (FISH) analysis at SMM diagnosis revealed 1q21 gain and 13q deletion as the cytogenetic abnormalities (Figure 1E). Based on these findings, the patient was diagnosed with SMM and managed with active surveillance in accordance with current guidelines.

To dissect cellular heterogeneity and track clonal changes, scRNA-seq and scBCR-seq were performed on BMMNC at three time points: initial diagnosis (T1), day 28 post-CAR-T cell therapy (T2), and day 180 post-CAR-T cell therapy (T3). Single-cell RNA and BCR libraries were generated using the 10× Genomics Chromium platform and sequenced on an Illumina NovaSeq X Plus. Data were processed using standard pipelines (Cell Ranger and Seurat), with Louvain clustering. Quality control excluded cells with UMI counts ≤1,000, detected genes <100 or >10,000, mitochondrial gene percentage ≥10%, or hemoglobin gene percentage ≥5%. scBCR-seq data were analyzed using scRepertoire,[7] and cell–cell communication was inferred using CellChat.[8] After integration and quality control, 24,732 high-quality cells were retained, comprising B-lineage, T/natural killer (T/NK)-lineage, and myeloid cells. Overall, T1 was primarily composed of B-ALL blasts. Post-CAR-T cell therapy (T2 and T3), blasts were eliminated, while plasma cells and T/NK cells increased (Figure 1F). Consistent with NGS-based Ig

A

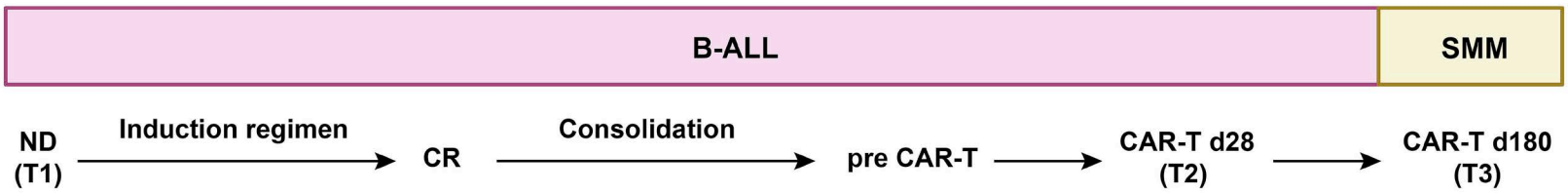

B

Characteristics	T1	T2	T3
WBC (×10⁹/L)	68.67	0.59	3.22
HGB (g/L)	115	69	108
PLT (×10⁹/L)	16	26	135
Albumin (g/L)	37.94	37.15	40.54
Globulin (g/L)	34.96	42.42	53.16
A/G ratio	1.09	0.88	0.76
Calcium (mmol/L)	2.22	2.21	2.4
Creatinine (μmol/L)	91	83.01	86.68
BUN (mmol/L)	5.54	4.94	4.84
eGFR (mL/min/1.73 m²)	80	89	85
BM smear			
Lymphoblasts	96.5%	0%	0%
Plasma cells	0.5%	20%	6.5%

C

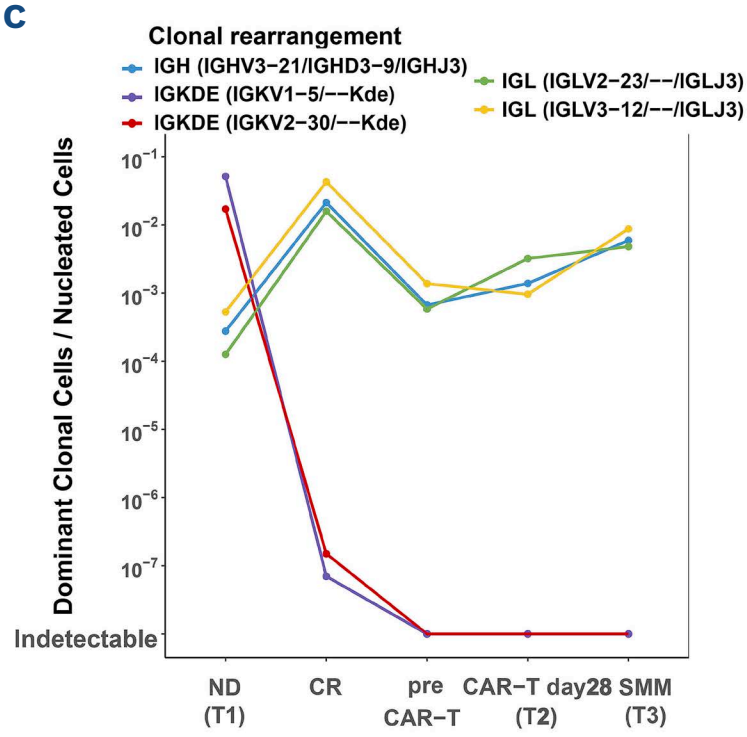

D

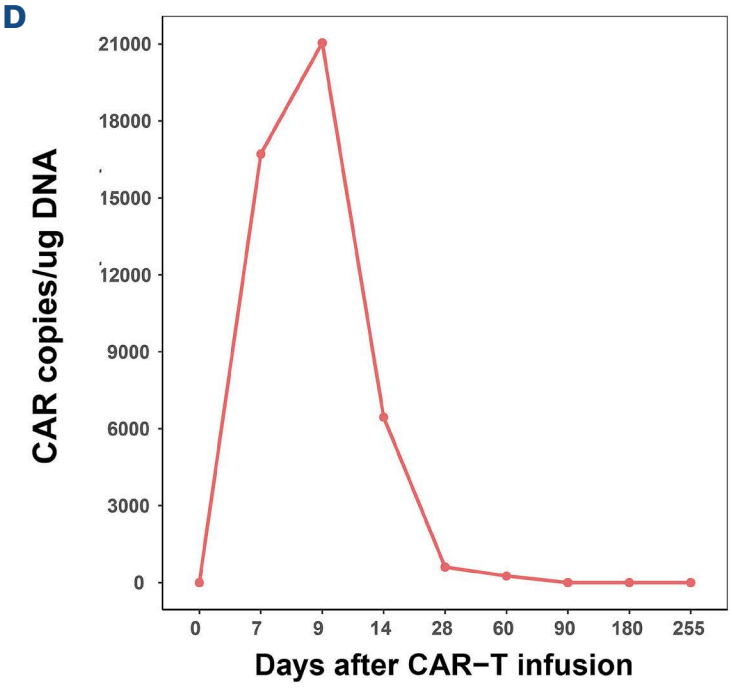

E

Probe / Locus	Cytogenetic abnormality	Positive cells (%)	Result
CDKN2C (1p32) / CKS1B (1q21)	1q21 gain	85.5	Positive
RB1 (13q14) / LAMP1 (13q34)	del(13q)	74.5	Positive
TP53 (17p13) / CEP17	del(17p)	Not detected	Negative
MYC (8q24)	MYC rearrangement	Not detected	Negative
IGH (14q32)	IGH rearrangement	Not detected	Negative

F

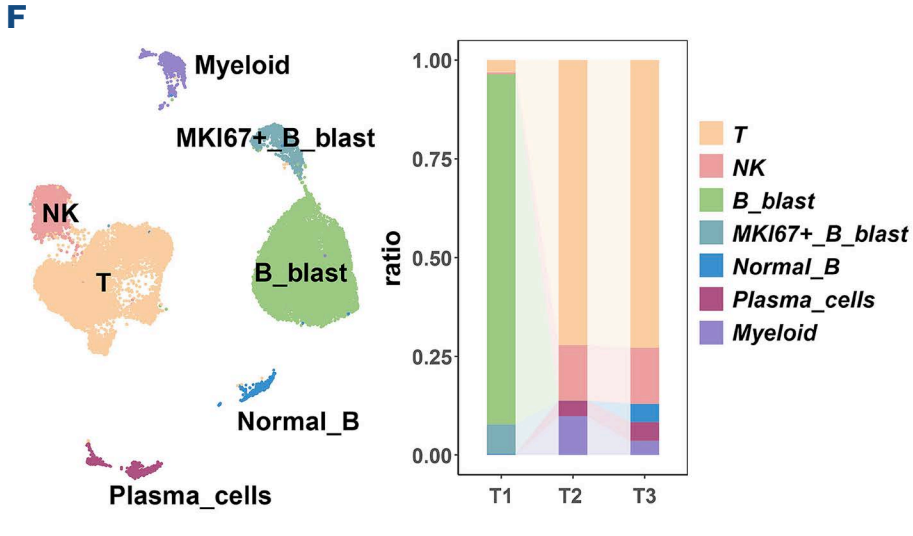

G

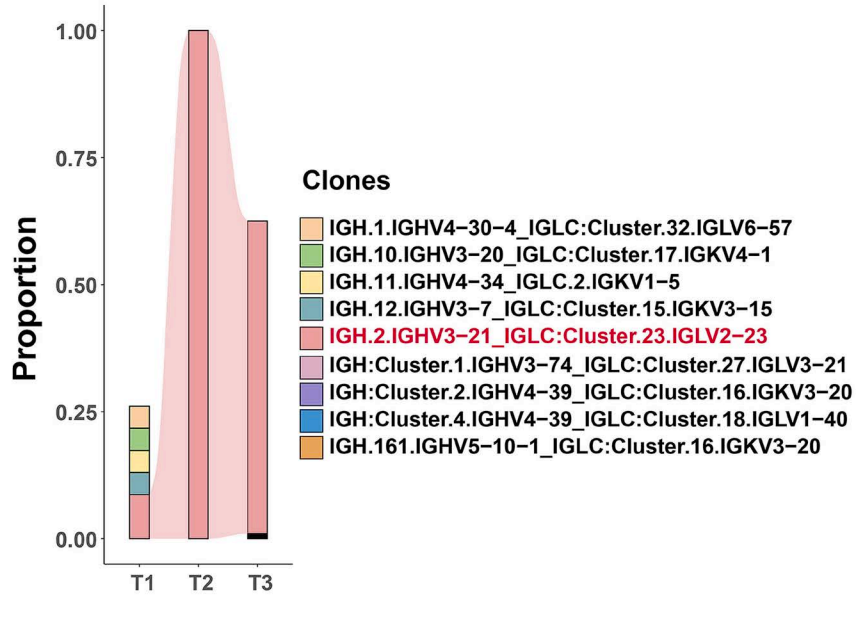

Continued on following page.

Figure 1. Longitudinal monitoring of disease evolution from B-cell acute lymphoblastic leukemia to smoldering multiple myeloma. (A) Schematic timeline of the patient's treatment course. ND (T1): newly diagnosed; CR: complete remission; pre-CAR-T: prior to chimeric antigen receptor T-cell therapy (CAR-T cell therapy); CAR-T d28 (T2): 28 days after CAR-T cell therapy; CAR-T d180 (T3): 180 days after CAR-T cell therapy. (B) Clinical parameters of the patient at three time points: T1 (diagnosis), T2 (day 28 post-CAR-T), and T3 (day 180 post-CAR-T). (C) Dynamics of clonal rearrangements across multiple time points, identified by Ig gene rearrangement analysis. (D) Kinetics of CAR-T cell copies in peripheral blood following CAR-T cell infusion. (E) Fluorescence *in situ* hybridization analysis of the patient at T3. (F) (Left) Uniform Manifold Approximation and Projection (UMAP) visualization of annotated cell clusters. (Right) Relative proportions of each cell type at T1, T2, and T3. Cell types were annotated using canonical markers: *CD3D/CD3E* (T cells), *NCAM1/FCGR3A* (natural killer [NK] cells), *CD79A/MS4A1* (B cells), *MZB1/SDC1* (plasma cells), and *CSF3R/LYZ* (myeloid cells). (G) Proportions of the dominant BCR clonotypes across T1, T2, and T3. A/G: albumin-to-globulin; B-ALL: B-cell acute lymphoblastic leukemia; BM: bone marrow; BUN; blood urea nitrogen; eGFR; estimated glomerular filtration rate; HGB: hemoglobin; PLT: platelet; SMM: smoldering multiple myeloma; WBC: white blood cell.

gene rearrangement analysis, scBCR-seq revealed that the dominant plasma cell clone harbored persistent *IGHV3-21* and *IGLV2-23* rearrangements (Figure 1G). Given the growing evidence of biological heterogeneity in SMM,[9] we next performed refined clustering of plasma cells. This analysis revealed three distinct subpopulations (Figure 2A), among which Plasma_cells_1 and Plasma_cells_2 were predominantly composed of a specific BCR clone (CARDGQNYDVLTGPTALDVW_CCSYAGSGTEWVF). Notably, *IGHV3-21* and *IGLV2-23* were highly expressed in these two subpopulations (Figure 2B).

To investigate the drivers of plasma cell expansion after CAR-T cell therapy, we analyzed post-treatment remodeling of the immune microenvironment. T-cell analysis revealed a distinct interferon-stimulated gene (ISG)$^+$ T subset that progressively expanded from T2 to T3 (Figure 2C). This population showed pronounced activation of the IFN response pathway (Figure 2D). We scored each T-cell subset using an ISG gene set[10] and found that ISG$^+$ T cells had the highest scores, with elevated *IFIT1, IFIT2,* and *IFIT3* expression (Figure 2E). Similarly, clustering analysis identified distinct NK subpopulations, among which the ISG$^+$ subset showed a marked increase in frequency at T3 compared with earlier time points (Figure 2F). Consistent with these observations, ISG scores were substantially higher in the ISG$^+$ NK cells (Figure 2G). Analysis of myeloid cell subsets revealed expansion of nonclassical monocytes at T3 (Figure 3A), which also displayed higher ISG scores and up-regulated ISG such as *IFITM1, IFITM2* and *IFITM3* (Figure 3B, C).

To evaluate the impact of ISG-high immune cell subsets on plasma cells, we performed cell-cell communication analysis. Nonclassical monocytes, ISG$^+$ T cells and ISG$^+$ NK cells exhibited interactions targeting plasma cells (Figure 3D). Specifically, nonclassical monocytes appeared to

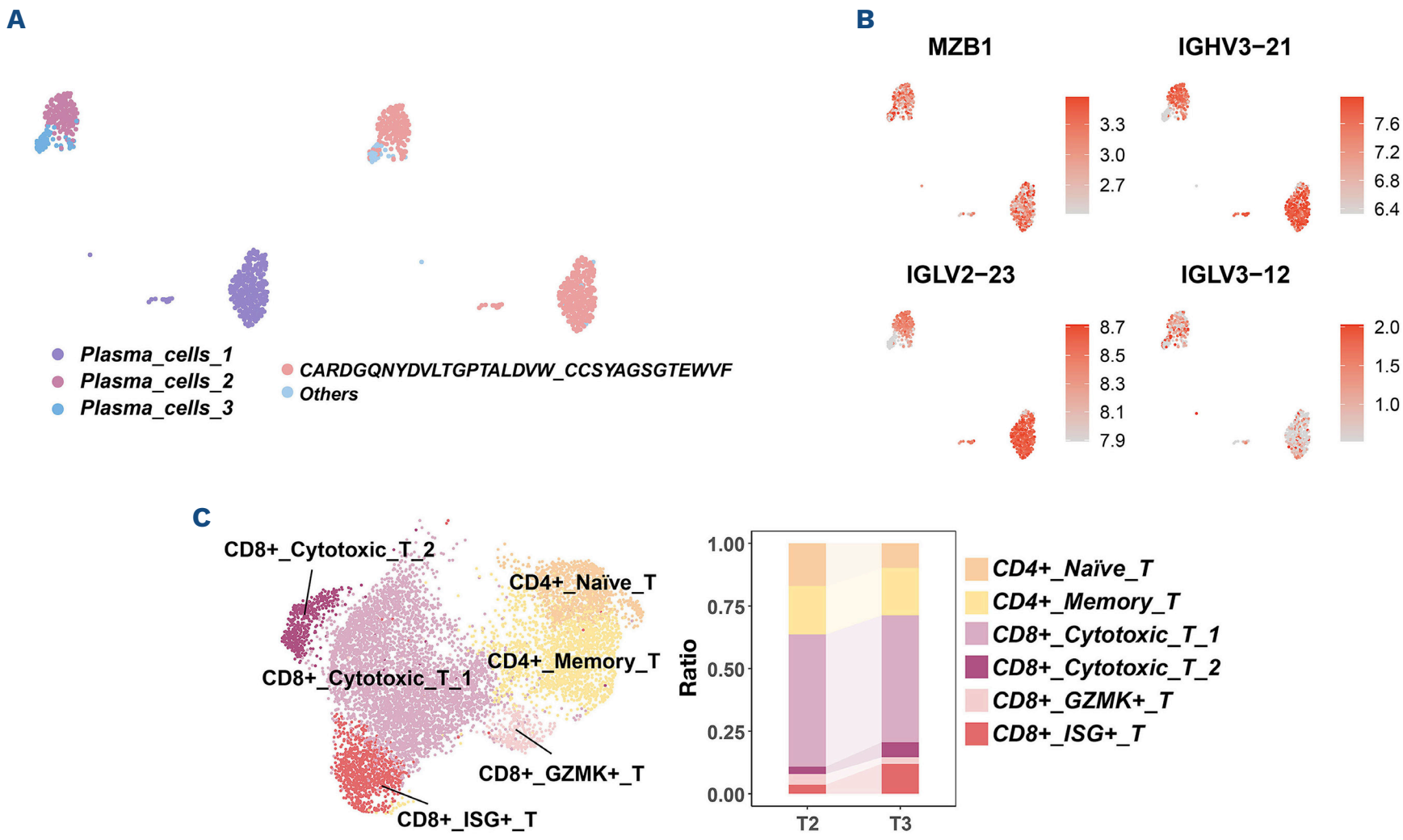

Continued on following page.

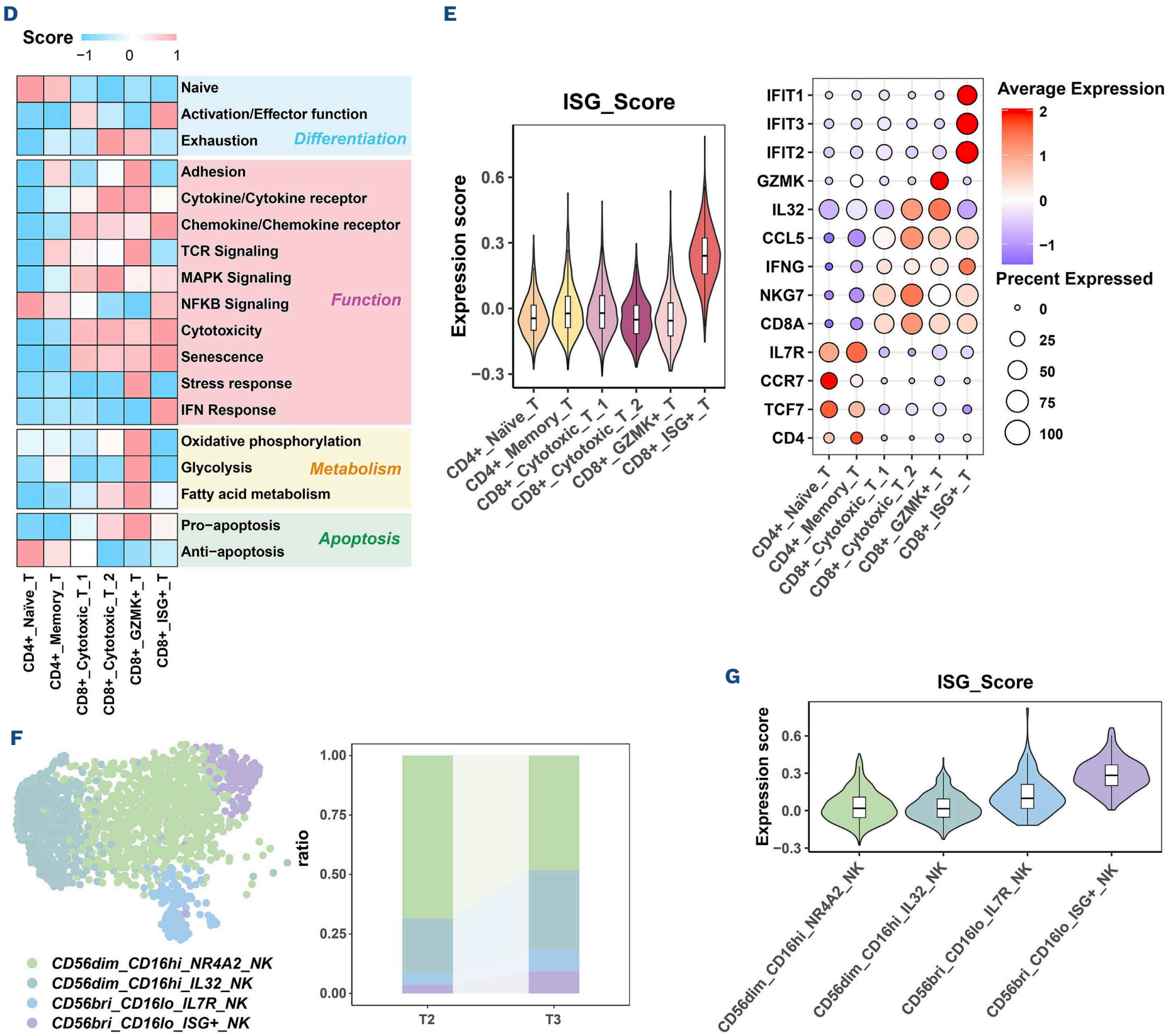

Figure 2. Dynamics of plasma cell, T cell, and natural killer cell subsets during chimeric antigen receptor T-cell therapy. (A) (Left) Uniform Manifold Approximation and Projection (UMAP) plot displaying three refined plasma cell subsets. (Right) The specific BCR clone identified by single-cell B-cell receptor sequencing (scBCR-seq) (CARDGQNYDVLTGPTALDVW_CCSYAGSGTEWVF) for each plasma cell subset. (B) Marker gene expression across plasma cell subsets. (C) (Left) UMAP plot displaying six refined T-cell subsets. (Right) Proportions of T-cell subsets at T2 (day 28 post-chimeric antigen receptor T-cell therapy [CAR-T cell therapy]) and T3 (day 180 post-CAR-T). (D) Pathway activity scores showing IFN-response enrichment in *CD8⁺_ISG⁺_T* cells. (E) (Left) Violin Plot of interferon-stimulated genes (ISG) score distributions across T-cell subsets. (Right) Dot plot of representative marker gene expression across T-cell subsets. (F) (Left) UMAP plot displaying four refined natural killer (NK) cell subsets. (Right) Proportions of NK cell subsets at T2 and T3. (G) Violin plot of ISG score distributions across NK cell subsets.

promote plasma cell survival through TNFSF13-TNFSF17 and TNFSF13B-TNFSF17 signaling, whereas ISG⁺ T and NK cells may facilitate plasma cell expansion via ITGB2-ICAM1 interactions (Figure 3E). Collectively, these findings indicated that CAR-T cell therapy induced an IFN-enriched immune microenvironment, in which ISG-high immune cell subsets paradoxically facilitated the expansion of plasma-cell clones (Figure 3F).

In this study, we report a B-ALL patient exhibiting notable clonal heterogeneity at diagnosis, with co-existing B-ALL and plasma cell clones. Following chemotherapy and CD19 CAR-T cell therapy, the B-ALL clones were effectively eradicated, whereas the plasma cell clones progressively expanded, ultimately manifesting as SMM. While secondary B-ALL has

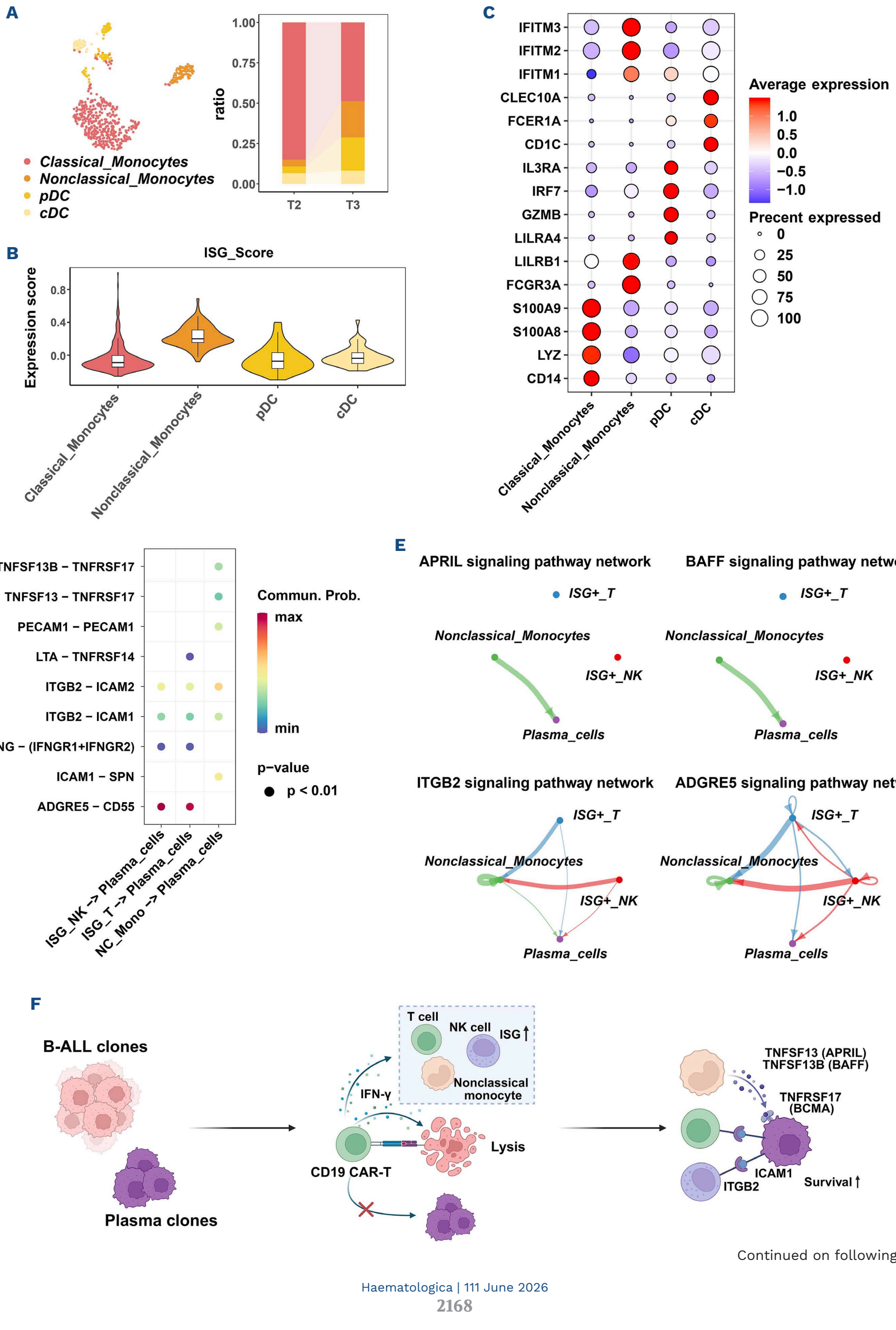

Continued on following page.

Figure 3. IFN-enriched immune remodeling and plasma-cell interactions after chimeric antigen receptor T-cell therapy. (A) (Left) Uniform Manifold Approximation and Projection (UMAP) plot displaying four refined myeloid cell subsets. (Right) Proportions of myeloid cell subsets at T2 (day 28 post-chimeric antigen receptor T [CAR-T] cell therapy) and T3 (day 180 post-CAR-T). (B) Violin plot of interferon-stimulated gene (ISG) score distributions across myeloid cell subsets. (C) Dot plot of representative marker gene expression across myeloid cell subsets. (D) Cell-cell communication analysis showing strong interactions from *Nonclassical_ Monocytes*, *CD8*$^{+}$*_ISG*$^{+}$*_T* cells and *CD56*^{bri}*_CD16*^{lo}*_ISG*$^{+}$*_NK* cells to plasma cells. NK: natural killer. (E) Network plot depicting signaling pathways mediating interactions from *Nonclassical_ Monocytes*, *CD8*$^{+}$*_ISG*$^{+}$*_T* cells and *CD56*^{bri}*_CD16*^{lo}*_ISG*$^{+}$*_NK* cells to plasma cells. (F) Schematic summary of an IFN-enriched bone marrow microenvironment in which IFN-responsive immune subsets support plasma-cell survival and expansion following CAR-T cell therapy. B-ALL: B-cell acute lymphoblastic leukemia.

been reported in MM patients,[11,12] to our knowledge, progression from B-ALL to MM following CAR-T cell therapy has not been previously reported.

Next-generation sequencing-based Ig gene rearrangement has become a powerful tool for MRD detection in B-ALL,[6] enabling longitudinal tracking of clonal Ig rearrangements. In this patient, five clonal Ig gene rearrangements were initially identified. Although NGS revealed temporal changes in clonal abundance, it could not identify the specific cellular origin of the expanding clones, potentially posing challenges for clinical management. Integration of longitudinal scRNA-seq and scBCR-seq, along with detailed single-cell clustering and annotation, demonstrated that the expanding IGH and IGL clones originated from plasma cells rather than residual B-ALL blasts. This cellular specification further highlights intrinsic B-lineage heterogeneity, potentially driven in part by dysregulated transcription factor activity.

Our single-cell transcriptomic analyses elucidate a mechanistic link between CAR-T cell therapy-induced immune remodeling and subsequent plasma cell expansion. Previous studies have shown that activation of the interferon (IFN) response is a hallmark of myeloma progression.[13,14] Following CAR-T cell infusion, distinct IFN-responsive immune subsets emerged, including ISG^{+} T cells, ISG^{+} NK cells, and IFN-activated nonclassical monocytes. These populations exhibited elevated expression of ISG, indicating that CAR-T cell therapy induced a sustained IFN-enriched immune microenvironment. In addition, IFN-responsive subsets such as nonclassical monocytes can provide critical proliferative signals to plasma cells through APRIL and BAFF,[15] suggesting a role in supporting plasma cell proliferation and survival. Concomitant depletion of CD19^{+} B-cell populations by CAR-T cell therapy, together with sustained IFN-driven cytokine support, may create a permissive ecological niche that favors the outgrowth of pre-existing, clinically occult plasma cell clones. While not implying a direct oncogenic effect, these findings suggest that CAR-T cell therapy associated immune remodeling may indirectly facilitate plasma cell clonal expansion, a hypothesis that warrants further experimental validation.

However, we acknowledge that this study is limited by its single-case design, which precludes establishing a causal relationship between CAR-T cell therapy, lymphodepletion, and the subsequent development of SMM. Although our longitudinal single-cell analyses provide insights into clonal evolution and immune remodeling, it remains unclear whether plasma cell expansion reflects therapy-induced changes or natural progression. In addition, the effects of IFN are complex and context-dependent. Future studies with larger cohorts are needed to validate these findings and to delineate the mechanisms underlying B-lineage clonal evolution after CAR-T cell therapy.

In summary, this case underscores the heterogeneity of B-lineage hematologic malignancies and documents the rare expansion of plasma cell clones in B-ALL post-CAR-T cell therapy. CAR-T cell therapy was associated with a sustained IFN-enriched immune microenvironment, accompanied by activation of IFN-responsive immune cells during plasma cell expansion. These findings highlight the need for clinicians to monitor B-cell clonal heterogeneity and inflammatory cytokine changes after CAR-T cell therapy.

Authors

Heye Yu,* Guangji Zhang,* Benfa Gong, Shouyun Li, Chengcai Guo, Yuntao Liu, Runxia Gu, Yingxi Xu, Gang An, Hui Wei, Min Wang, Qing Rao, Wenbing Liu, Jianxiang Wang and Shaowei Qiu

State Key Laboratory of Experimental Hematology, National Clinical Research Center for Blood Diseases, Tianjin Key Laboratory of Cell Therapy for Blood Diseases, Haihe Laboratory of Cell Ecosystem, Institute of Hematology & Blood Diseases Hospital, Tianjin Institutes of Health Science, Chinese Academy of Medical Sciences & Peking Union Medical College (CAMS&PUMC), Tianjin, China

**HY and GZ contributed equally as first authors.*

Correspondence:
W. LIU - liuwenbing@ihcams.ac.cn
J. WANG - wangjx@ihcams.ac.cn
S. QIU - qiushaowei@ihcams.ac.cn

https://doi.org/10.3324/haematol.2025.300240

Received: November 19, 2025.
Accepted: February 4, 2026.
Early view: February 12, 2026.

Disclosures

No conflicts of interest to disclose.

Contributions

HY and GZ collected, verified, and interpreted patient information, and drafted the manuscript; BG, SL, CG, YL, RG, YX, GA, HW, MW and QR revised the manuscript; WL, JW and SQ designed the research, and critically reviewed and revised the final draft. All authors read and approved the final manuscript for publication.

Acknowledgments

We thank the patient and family for their participation. We also thank Yujiao Jia and Jiao Chang at the Institute of Hematology & Blood Diseases Hospital, CAMS&PUMC for their assistance with the interpretation of bulk NGS BCR-seq data.

Funding

This work was supported by the National Natural Science Foundation of China (82341213, 82570215), the CAMS Innovation Fund for Medical Sciences (2024-I2M-ZH-015, 2024-I2M-TS-023, 2025-I2M-C&T-B-075), and a Tianjin Municipal Science and Technology Commission Grant (23JCYBJC01050).

Data-sharing statement

The raw sequence data reported in this paper have been deposited in the Genome Sequence Archive in National Genomics Data Center, China National Center for Bioinformation / Beijing Institute of Genomics, Chinese Academy of Sciences (GSA-Human: HRA011090) and are publicly accessible at https://ngdc.cncb.ac.cn/gsa-human.

References

1. Rampotas A, Roddie C. The present and future of CAR T-cell therapy for adult B-cell ALL. Blood. 2025;145(14):1485-1497.
2. Coorens THH, Collord G, Treger TD, et al. Clonal origin of KMT2A wild-type lineage-switch leukemia following CAR-T cell and blinatumomab therapy. Nat Cancer. 2023;4(8):1095-1101.
3. Xia X, Yang Z, Lu Q, et al. Reshaping the tumor immune microenvironment to improve CAR-T cell-based cancer immunotherapy. Mol Cancer. 2024;23(1):175.
4. Zhang Y, Wang S, Zhang J, et al. Elucidating minimal residual disease of paediatric B-cell acute lymphoblastic leukaemia by single-cell analysis. Nat Cell Biol. 2022;24(2):242-252.
5. Gong X, Liu W, Liu Y, et al. Olverembatinib combined with venetoclax and reduced-intensity chemotherapy for adult newly diagnosed Philadelphia chromosome-positive acute lymphoblastic leukemia: a single-center, single-arm, phase 2 trial. Leukemia. 2025;39(8):1838-1847.
6. Chen H, Gu M, Liang J, et al. Minimal residual disease detection by next-generation sequencing of different immunoglobulin gene rearrangements in pediatric B-ALL. Nat Commun. 2023;14(1):7468.
7. Borcherding N, Bormann NL, Kraus G. scRepertoire: an R-based toolkit for single-cell immune receptor analysis. F1000Res. 2020;9:47.
8. Jin S, Guerrero-Juarez CF, Zhang L, et al. Inference and analysis of cell-cell communication using CellChat. Nat Commun. 2021;12(1):1088.
9. Maura F, Bergsagel PL, Ziccheddu B, et al. Genomics define malignant transformation in myeloma precursor conditions. J Clin Oncol. 2026;44(3):188-199.
10. Chu Y, Dai E, Li Y, et al. Pan-cancer T cell atlas links a cellular stress response state to immunotherapy resistance. Nat Med. 2023;29(6):1550-1562.
11. Barnell EK, Skidmore ZL, Newcomer KF, et al. Distinct clonal identities of B-ALLs arising after lenolidomide therapy for multiple myeloma. Blood Adv. 2023;7(2):236-245.
12. Roerden M, Hensen L, Besemer B, et al. Dual anti-CD19/22 and anti-BCMA CAR-T cell therapy in a patient with multiple myeloma and secondary B-ALL. Blood Adv. 2025;9(24):6340-6344.
13. Zavidij O, Haradhvala NJ, Mouhieddine TH, et al. Single-cell RNA sequencing reveals compromised immune microenvironment in precursor stages of multiple myeloma. Nat Cancer. 2020;1(5):493-506.
14. Cheng Y, Sun F, Alapat DV, et al. Multi-omics reveal immune microenvironment alterations in multiple myeloma and its precursor stages. Blood Cancer J. 2024;14(1):194.
15. Moreaux J, Legouffe E, Jourdan E, et al. BAFF and APRIL protect myeloma cells from apoptosis induced by interleukin 6 deprivation and dexamethasone. Blood. 2004;103(8):3148-3157.